 FDMP, vol.1, no.1, pp.21-31, 2005

On the Three-Dimensional Instability of Thermocapillary Convection in Arbitrarily Heated Floating Zones in Microgravity Environment

A.Yu. Gelfgat[1], A. Rubinov[2], P.Z. Bar-Yoseph [2] and A. Solan [2]

Abstract: The three-dimensional instability of the thermocapillary convection in cylindrical undeformable floating zones heated laterally is studied numerically. Different types of the boundary conditions, including radiation heating, linearized radiation and prescribed heat flux are used in the calculation. Stability diagrams showing the Prandtl number dependence of the critical Marangoni numbers that represent the thermocapillary forcing for different heating conditions are reported. It is shown that the primary instability of initially axisymmetric thermocapillary flows is defined mainly by the total amount of heat supplied through the heated side surface. The way in which the heat is supplied has a less significant effect on the onset of instability.

keyword: crystal growth, microgravity, hydrodynamic stability

1 Introduction

Crystal growth from a melt in the space environment in the absence of gravity-driven buoyant convection is regarded as a promising method to achieve more stable and uniform crystal growth conditions that would result in better crystal quality. When the buoyancy force becomes negligibly small, convection may be driven by the thermocapillary force that results from a surface tension gradient due to temperature difference. The instability of such thermocapillary flows in floating zone and liquid bridge crystal growth configurations, in particular in relation to the space-flight environment, is a widely known phenomenon studied extensively experimentally and numerically (Lappa 2004). The amount of literature on this subject is very extensive and cannot be reviewed within the present paper. Generally, the problems considered by different authors can be divided into two categories. The first group of studies considers the thermocapillary convection between two differentially heated isothermal disks with adiabatic sidewall. The experimental studies of this configuration were performed by Preisser et al. (1983), Albanese et al. (1995), Muehlner et al. (1997), Sumner et al. (2001), Majima et al. (2001), Hibiya et al. (2002), Kamotani et al. (2003), Nishimura et al. (2005) and numerical studies by Shen (1990), Kuhlmann & Rath (1993), Wanshura et al. (1995), Chen et al. (1997), Levenstam et al. (2001), Imaishi et al. (2001), Sumner et al. (2001), Lappa et al. (2001), Yasuhiro et al. (2004), Melnikov et al. (2005), and Zeng et al. (2005), and other works referred in these papers. This model is the simplest possible, but cannot completely simulate the floating zone process where the liquid zone is heated from the side. Some of the authors argued that this model describes a "half-zone" model, however this would imply unphysical boundary conditions at the midplane of the whole liquid zone.

Experimental studies of thermocapillary convection with side heating of the liquid zone are more difficult, especially for non-transparent low-Prandtl-number fluids like molten semiconductors. These studies are usually restricted to the measurements of the temperature (e.g., Hsieh & Lan, 1996; Yang & Kou, 2001), or a-posteriori analysis of grown crystals (e.g., Cröll et al., 1998; Dold, 2004; Kimura et al., 2004). The correct thermal boundary condition at the side surface of the floating zone should account for the heating by radiation. This boundary condition was accounted for by Munakata & Tanasawa (1999), Lan & Chian (2001), and Lan (2003). The non-linearity introduced by the radiation boundary condition causes numerical difficulties, and other authors tried to simplify it either by linearization (Minakuchi et al., 2004) or by imposing a given heat flux at the side surface (Kasperski et al., 2000; Bennacer et al., 2002; Lappa, 2003 & 2005). In particular, Bennacer et al. (2002) studied how different axial profiles of the heat flux affect the flow patterns and transition from axisymmetric

[1] School of Mechanical Engineering, Faculty of Engineering, Tel-Aviv University, Israel.
[2] Computational Mechanics Laboratory, Faculty of Mechanical Engineering, Technion - Israel Institute of Technology

steady to axisymmetric oscillatory flow.

In the present paper we study how different boundary conditions defined on the lateral surface of the floating zone can affect the three-dimensional instability of initially axisymmetric flow. This problem was not addressed in the previous studies and is essential for the understanding how the non-linear radiative boundary condition can be simplified without a loss of essential flow features. The three-dimensional instability of liquid bridges located between isothermal differentially heated disks was addressed by several authors (Shen, 1990; Kuhlmann & Rath, 1993; Wanshura et al., 1995; Chen et al., 1997; Levenstam et al., 2001), however for the side heated zones the axisymmetry – three-dimensional transition was addressed mainly by the time-dependent solutions of fully 3D problems (e.g., Lappa, 2003 and 2005). The only stability study for the side-heated zones was performed by Walker et al. (2003) for a parabolic heat flux at the side wall. Here we report stability diagrams for the axisymmetric – three-dimensional transition of the side heated undeformable floating zones, and consider fully radiative, linearized and heat flux boundary conditions. We compare the onset of the three-dimensional instability for the three types of the boundary condition, and for heat fluxes of different shape defined at the side surface. These comparisons lead us to the conclusion that the instability of such a thermocapillary flow is defined mainly by the total amount of heat supplied through the side surface. The shape of the heat flux profile, as well as more precise accounting for the radiative heating can only slightly change the flow patterns and stability limits.

The study is performed numerically using the finite volume discretization. The steady state and stability analysis are performed in the same way as in Rubinov et al. (2004) and Gelfgat et al. (2005).

2 Formulation of the problem.

We consider the three-dimensional stability of an axisymmetric thermocapillary flow in an undeformable cylindrical floating zone. The fluid is located in a cylindrical domain $0 \le z \le H$ and $0 \le r \le R$. The upper and lower boundaries $z=0$ and $z=H$ are rigid and isothermal. The side boundary $r=R$ is exposed to an external heater, whose properties will be defined below, and to the action of the thermocapillary force. The problem is sketched in Fig. 1.

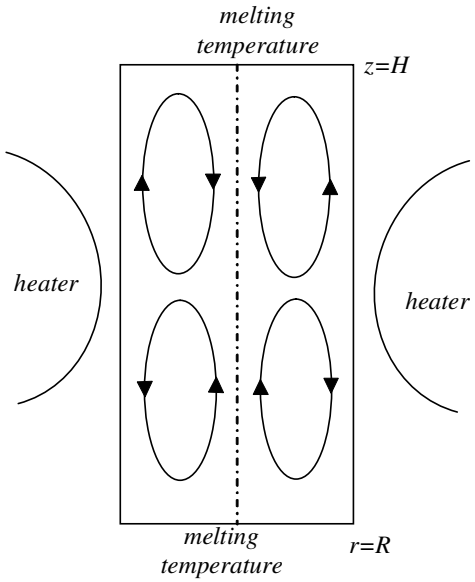

Figure 1 : Sketch of the problem

The flow is governed by the dimensionless momentum, continuity and energy equations in the Boussinesq approximation written in the cylindrical coordinates (r,θ,z)

$$\frac{\partial \mathbf{v}}{\partial t} + (\mathbf{v}\cdot\nabla)\,\mathbf{v} = -\nabla p + \Delta \mathbf{v}, \tag{1}$$

$$\nabla \cdot \mathbf{v} = 0, \tag{2}$$

$$\frac{\partial T}{\partial t} + (\mathbf{v}\cdot\nabla)\,T = \mathrm{Pr}^{-1}\Delta T \tag{3}$$

with the no-slip boundary and isothermal boundary conditions at the lower and upper boundaries

$$\mathbf{v} = 0, \quad \mathrm{T} = 0 \qquad \text{at } z = 0 \text{ and } A \tag{4}$$

and the tangent stress balance at the side boundary

$$v_r = 0, \;\; \frac{\partial v_z}{\partial r} = -Mn\frac{\partial T}{\partial z}, \;\; \frac{\partial v_\theta}{\partial r} = -Mn\frac{\partial T}{\partial \theta} \quad \text{at } r = 1 \tag{5}$$

Here $\mathbf{v}=(\mathrm{v}_r,\mathrm{v}_\theta,\mathrm{v}_z)$, p, and T are the velocity, pressure and temperature of the fluid, respectively; $Pr=\nu/\kappa$ is the Prandtl number, $Ma = -\gamma\left(\tilde{T}_h - \tilde{T}_m\right)R/\nu\kappa$ is the Marangoni number and the dimensionless parameter $Mn=Ma/Pr$ is interpreted sometimes as thermocapillary Reynolds number; ν is the kinematic viscosity, κ is the thermal diffusivity, $\tilde{T}_h$ is the characteristic temperature of the heater, which is defined here by the heater

hottest point, and $\tilde{T}_m$ is the melting temperature. It is assumed that the surface tension coefficient α decreases linearly with the increase of the temperature, so that $\gamma = \partial\alpha/\partial\tilde{T}$is a negative constant ($\tilde{T}$ is the dimensional temperature). The temperature is rendered dimensionless by $T = \left(\tilde{T} - \tilde{T}_m\right)/\left(\tilde{T}_h - \tilde{T}_m\right)$. The aspect ratio of the zone is defined as $A = H/R$. The characteristic scales of length, time, velocity and pressure are R, R^2/ν, ν/R, and $\rho\nu^2/R^2$, respectively.

The thermal boundary conditions at the side surface of the fluid is imposed by a radiative heater whose temperature $\tilde{T}_{heater}(\tilde{z})$ can be a function of $\tilde{z}$, where $\tilde{z}$ is a dimensional coordinate. In dimensional form, where $\tilde{r}$ and $\tilde{z}$ are dimensional coordinates

$$-\lambda\frac{\partial\tilde{T}}{\partial\tilde{r}} = \sigma\varepsilon F_\varepsilon(\tilde{z})\left[\tilde{T}_R^4 - \tilde{T}_{heater}^4(\tilde{z})\right],\ \tilde{T}_R = T(R,\theta,\tilde{z}) \quad (6)$$

where λ is the thermal conductivity, ε is the absorbtivity coefficient and σ is the Stefan-Boltzmann constant. The shape factor $F_\varepsilon(\tilde{z})$ is defined by the location of a surface point with respect to the heater. Since the present analysis is not related to any specific configuration we assume $F_\varepsilon(\tilde{z}) = 1$. In the dimensionless form the boundary condition (6) reads

$$\frac{\partial T}{\partial r} = -Rd\left[\left(T + \frac{T_m}{T_h - T_m}\right)^4 - \left(\frac{\tilde{T}_{heater}(z)}{T_h - T_m}\right)^4\right] \quad \text{at } r\text{=}1 \quad (7)$$

where $Rd = \varepsilon\sigma R\left(T_h - T_m\right)^3\Big/\lambda$ is the radiation number. Equation (7) can be easily rewritten as

$$\frac{\partial T}{\partial r} = -Rd\left[\left(T + \hat{T}_m\right)^2 + \hat{T}_{heater}^2(z)\right]\times \quad (8)$$
$$\left[\left(T + \hat{T}_m\right) + \hat{T}_{heater}(z)\right]\left[\left(T + \hat{T}_m\right) - \hat{T}_{heater}(z)\right]$$

where $\hat{T}_m = T_m/(T_h - T_m)$ and $\hat{T}_{heater}(z) = \tilde{T}_{heater}(z)/(T_h - T_m)$. Assuming that $\left(T + \hat{T}_m\right) \ll \hat{T}_{heater}(z)$ the non-linear boundary condition (8) can be replaced by

$$\frac{\partial T}{\partial r} = Rd \quad \hat{T}_{heater}^4(z) = q(z) \quad \text{at } r\text{=}1 \quad (9)$$

On the other hand, assuming that the temperature of the heater and of the melt surface change slowly along the z-direction we can introduce

$$T_{eff}^3 \approx \left[\left(T + \hat{T}_m\right)^2 + \hat{T}_{heater}^2\right]\left[\left(T + \hat{T}_m\right) + \hat{T}_{heater}\right] \quad (10)$$

and consider a linearized boundary condition considered by Minakuchi et al. (2004)

$$\frac{\partial T}{\partial r} = -Bi\left[\left(T + \hat{T}_m\right) - \hat{T}_{heater}(z)\right] \quad \text{at } r\text{=}1 \quad (11)$$

where $Bi = Rd\ \hat{T}_{eff}^3$ is the effective Biot number.

In the following we calculate the axisymmetric steady flows governed by equations (1)-(5) and the boundary conditions (7), (9) or (11). Then we study the linear stability of the calculated flows with respect to infinitesimal three-dimensional perturbations. Assuming that $\mathbf{V}(r,z) = \{U(r,z), V(r,z), W(r,z)\}$, $P(r,z)$ and $T(r,z)$ is the calculated axisymmetric basic flow and taking into account the periodicity in the azimuthal direction the perturbations of the velocity, pressure and the temperature are represented as

$$\{\mathbf{v}, p, \tau\} = \sum_{k=-\infty}^{k=\infty}\{\mathbf{v}_k(r,z), p(r,z), \tau(r,z)\}\exp(\Lambda t + ik\theta). \quad (12)$$

Here Λ is the growth rate and k is the azimuthal wavenumber, which plays the role of an additional integer parameter. It is a well-established fact that the linear stability problem separates for each value of k. Thus the stability problem reduces to the sequence of the eigenvalue problems

$$\Lambda\mathbf{v}_k = -(\mathbf{v}_k\cdot\nabla)\mathbf{V} - (\mathbf{V}\cdot\nabla)\mathbf{v}_k - \nabla p_k + \Delta\mathbf{v}_k, \quad (13)$$

$$\nabla\cdot\mathbf{v}_k = 0, \quad (14)$$

$$\Lambda\tau_k = -(\mathbf{v}_k\cdot\nabla)T - (\mathbf{V}\cdot\nabla)\tau_k + \mathrm{Pr}^{-1}\Delta\tau_k \quad (15)$$

with the corresponding linearized boundary conditions, which should be solved sequentially for each value of k. The basic axisymmetric flow is unstable when $Real(\Lambda) > 0$. The equation $Real[\Lambda(Mn_m, k)] = 0$ defines the marginal values of the parameter Mn for each k. The critical value of the governing parameter is defined by $Mn_{cr} = \min_k[Mn_m(k)]$.

3 Numerical technique

The governing equations are discretized using the finite volume approach. The basic steady axisymmetric flows are calculated by Newton iteration with complete calculation of the Jacobian matrix. The BICGstab(2) algorithm is used to solve the system of linear equations at

each Newton iteration. The parameter continuation is applied where necessary.

Assuming that the flow region is mapped onto a certain grid and that the discretization at a grid node (r_i, z_j) is known, the eigenvalue problem (13)-(15) is reduced to a generalized algebraic eigenvalue problem, which can be expressed in the following form

$$\Lambda \mathbf{v}_{ij} = -\left[(\mathbf{v}\cdot\nabla)\,\mathbf{V}\right]_{ij} - \left[(\mathbf{V}\cdot\nabla)\,\mathbf{v}\right]_{ij} - [\nabla p]_{ij} + [\Delta \mathbf{v}]_{ij},$$

$$[\nabla\cdot\mathbf{v}]_{ij} = 0,$$

$$\Lambda \tau_{ij} = -\left[(\mathbf{V}\cdot\nabla)\,\tau\right]_{ij} - \left[(\mathbf{v}\cdot\nabla)\,T\right]_{ij} + Pr^{-1}\,[\Delta\tau]_{ij}. \tag{16}$$

Here $[\cdot]_{ij}$ denote the discretization at a node. Equations (16) apply to all the inner nodes. Additional equations discretizing the boundary conditions must be supplied at all the boundary nodes.

The complete set of the linearized equation leads to the generalized algebraic eigenproblem

$$A\mathbf{x} = \lambda B\mathbf{x} \tag{17}$$

where $\mathbf{x}$ is the vector of unknowns, and A and B are complex matrices. Due to the continuity equation and the boundary conditions the matrix B is singular, so that problem (17) cannot be transformed into a standard eigenvalue problem. It is solved by the Arnoldi iteration in the shift-and inverse-mode

$$(A-\beta B)^{-1} B\mathbf{x} = \mu\mathbf{x}, \quad \mu = 1/(\Lambda-\beta) \tag{18}$$

where β is a complex shift. It should be noted that this approach succeeds when the shift β, which can be complex, is chosen close to the leading eigenvalue Λ. It is an easy task for those problems for which the estimate of Λ is known. However, it is an additional difficulty for each new problem where no information on the stability properties of the flow is available.

Each Arnoldi iteration requires the solution of the linear equations system $(A–\beta B)\mathbf{x}=\mathbf{b}$. The usual approach is an iterative solution of these equations. The iterative solution usually requires too many iterations, because the right hand side vector $\mathbf{b}$ changes completely from one iteration to another, so that no good initial guess for the solution can be supplied. As in Gelfgat et al (2005) we use another approach, in addition to the iterative one, which constructs the LU decomposition of the sparse matrix $(A–\sigma B)$. This consumes much more computer memory and a certain amount of CPU time for the calculation of the LU decomposition. At the same time, the consequent Arnoldi iterations become fast, which allows us to calculate quite many leading eigenvalues. The number of the eigenvalues in different runs varies from 10 to 100. This approach can fail when the matrix is ill-conditioned. Since the iterations can diverge as well, the use of two different linear solvers makes our numerical approach more flexible. In all the calculations the finite volume grid was stretched near the side, upper and lower boundaries. Examples of the test calculations are shown in Tables 1 and 2. Table 1 shows the convergence and the comparison with the calculation of Bennacer et al. (2002). In this case we consider the liquid bridge with aspect ratio A =2 and the boundary conditions (9). Following Bennacer et al. (2002) the dimensionless heat flux is defined as $q(z) = \left[1-(1-z)^2\right]^2$. It follows that the use of the grid with 120 nodes in the axial and 60 nodes in the radial direction yields a satisfactory result, which compares well with the results of Bennacer et al. (2002) obtained on the much finer grid 300×150. As a rule, finer grids are needed to reach the convergence of the critical numbers. Thus, for the following stability calculations with the aspect ratio A =1 we use a 100×100 grid.

Table 1 : Convergence study A = 2, Pr = 1, Mn=3000, with the boundary conditions (9), $q(z) = \left[1-(1-z)^2\right]^2$.

$N_z \times N_r$	T_{max}	W_{max}
45×30	0.2937	109.65
60×35	0.3039	106.28
80×40	0.3036	104.20
120×60	0.3034	103.01
180×90	0.3034	102.81
Result of Bennacer et al. (2002), grid 300×150	0.3034	102.77

Table 2 shows the comparison of the calculated critical Mn numbers and the corresponding critical frequencies for a rather popular problem that considers a liquid bridge between two differentially heated isothermal disks with a thermally insulated sidewall. The comparison is made with the works of Chen et al. (1997), Wanshura

Table 2 : Critical parameters for Marangoni convection in a liquid bridge with differentially heated end boundaries, $A=1$. [1] – Chen et al., (1997), [2] – Wanshura et al. (1995), [3] – Levenstam et al. (2001). [4] – Imaishi et al. (2001)

Pr	k	Mn_{cr}					ω_{cr}				
		present	[1]	[2]	[3]	[4]	present	[1]	[2]	[3]	[4]
0	2	**1784**	1784	1793	1793	1958	**0**	0	0	0	0
0.01	2	**1896**	1892	1899	1901	2080	**0**	0	0	0	0
0.02	2	**2057**	2054	2062	2062	2202	**0**	0	0	0	0
0.05	2	**3520**	3528	3434	3522	-	**0**	0	0	0	-
0.06	3	**13270**	-	-	13251	-	**171**	-	-	179	-
0.07	2	**18319**	-	-	18302		**54.8**	-	-	54.3	-
0.1	2	**16130**	16201	-	16094	-	**74.9**	450(3)	-	74.2	-
0.2	3	**13290**	13278	-	13275	-	**396**	391	-	393	-
0.7	3	**7575**	7566	9608	7570	-	**187.4**	187.1	197.7	187	-
1.0	2	**2533**	2532	2539	2551	-	**64.2**	64.7	63.2	65.0	-
4.0	2	**997**	995	1047	1002	-	**28.3**	28.3	27.9	28.5	-

et al. (1995), Levenstam et al. (2001) and Imaishi et al. (2001) for different Prandtl numbers and shows a good agreement, especially with the results of Levenstam et al. (2001).

An additional comparison based on from the study of Cröll et al. (1998). The calculations were performed for Pr=0.04, A =0.8 and the boundary condition (9) with $q(z) = z\left(1-z/A\right)$. The axisymmetric – three-dimensional transition was found by Cröll et al. (1998) using a fully 3D calculation to take place for $Ma>100$ so that the resulting three-dimensional flow remains steady. The present result is a steady bifurcation at Ma_{cr}=112 and k_{cr}=2.

4 Results

The present calculations were performed for the fixed value of the aspect ratio $A=1$. The range of the Prandtl number values was chosen as $0<Pr\leq 0.1$, which covers the Prandtl numbers that are typical for liquid semiconductors. Examples of steady axisymmetric flow patterns are given in Fig.2. It is seen that independently of the type of thermal boundary condition imposed at the side surface the flow inside a symmetrically heated zone consists of two main vortices located near the surface and two weak recirculation vortices located closer to the axis. Note, that in all the cases shown the shape of the streamlines remains similar. At larger Prandtl numbers (Fig. 2c) convection makes the temperature along the surface almost uniform which is followed by a noticeable deformation of the isotherms inside the fluid volume. This change of the temperature distribution is characteristic for all the boundary conditions considered.

Figure 3 illustrates how the stability analysis is performed. In the reported case we considered the boundary condition (11) with the parabolic outside temperature profile $\hat{T}_{heater}(z)-\hat{T}_m = 4z(1-z)$ similar to the one considered by Gelfgat, Bar-Yoseph and Solan (2000). The marginal stability curves are calculated subsequently for different values of the azimuthal wavenumber k. The four of these that have minimal marginal values of Mn are shown in Fig. 3. The stability limit is given by the lower envelope of all the marginal curves. It is seen that the most unstable azimuthal mode at low Prandtl numbers corresponds to $k=3$. This mode is steady, i.e., the imaginary part of the leading eigenvalue of the linear stability problem is zero. At larger Prandtl numbers, approximately at Pr=0.07, it is replaced by the oscillatory mode $k=1$. The dimensionless circular frequency of the perturbation varies between 410 and 430. At $Pr>0.1$ the mode $k=2$ tends to be the most unstable.

The lower envelopes of the marginal stability curves, which form the neutral curves of the stability diagram, are shown in Figs 4 and 5. Transitions between the azimuthal modes $k=1$ and $k=3$ are shown by hairlines. Figure 4 shows the neutral curves for different Biot numbers of the boundary condition (11). Figure 5 shows the neutral curves for three different heating laws.

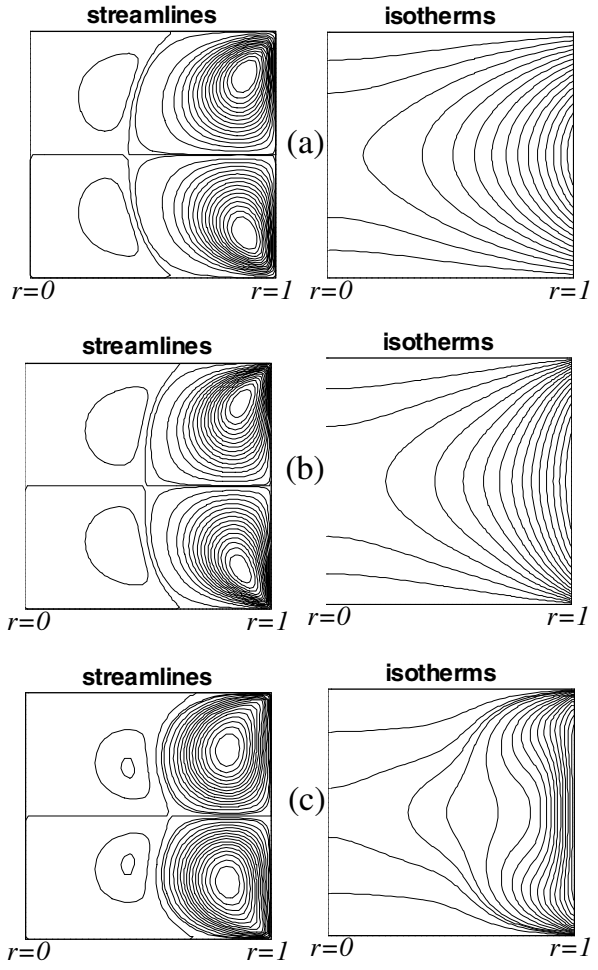

Figure 2 : Examples of the flow patterns, A =1. (a) Pr=0.01, Mn=6200, boundary condition (9) with $q(z) = 4z(1-z)$; (b)Pr=0.05, Mn=2×10^5, boundary condition (9) with T_{heater}=1, (c) boundary condition (11) Pr=0.08, Mn=$2.4\times10^5$with $\hat{T}_{heater}(z) - \hat{T}_m = 4z(1-z)$.

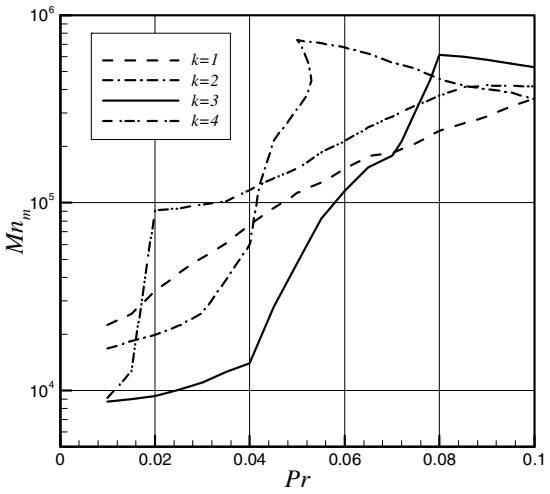

Figure 3 : Marginal stability curves for different azimuthal modes. Calculation for A=1, boundary condition (11) with Bi=1 and $\hat{T}_{heater}(z) - \hat{T}_m = 4z(1-z)$.

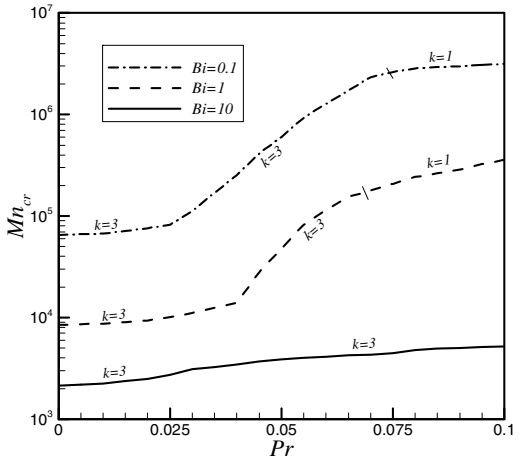

Figure 4 : Stability diagrams for A =1, and boundary conditions (11) with $\hat{T}_{heater}(z) - \hat{T}_m = 4z(1-z)$ for different Biot numbers.

The values of Mn_{cr} strongly differ for different Biot numbers (Fig. 4), as well as for different heating laws (Fig. 5). At the same time, we observe that at each neutral curve the azimuthal mode k =3 is the most unstable for low Prandtl numbers and is replaced by the mode k =1 when the Prandtl number is increased. Moreover, the modes k =3 are always steady, while the modes k =1 are oscillatory. A closer look at the most unstable perturbations (not shown here) reveals a similarity between the perturbations belonging to the same azimuthal mode. All this allows us to assume that there is a strong similarity in the axisymmetric – three-dimensional transition of such thermocapillary flows, which occurs due to the same physical mechanism independently of the heating law prescribed at the side surface. Apparently, a critical amount of heat needs to be supplied to trigger the instability, however the way in which this heat is supplied seems to be less important.

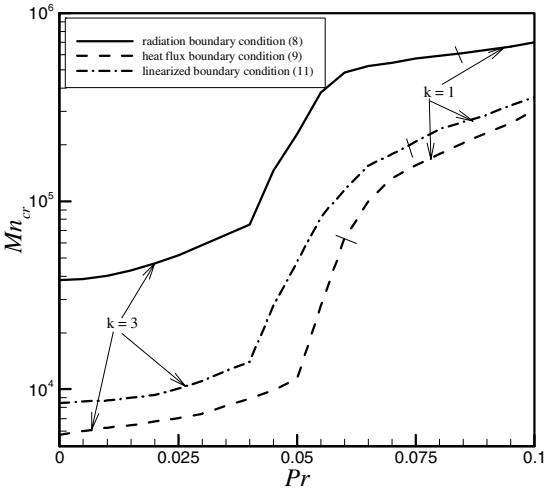

Figure 5 : Neutral stability curves for A =1 and different thermal boundary conditions at the surface: radiation boundary condition (8) with $\hat{T}_{heater} = 1$, linearized boundary condition (11) with Bi=1 and $\hat{T}_{heater}(z) - \hat{T}_m = 4z(1-z)$, and prescribed heat flux (9) with $q(z) = 4z(1-z)$.

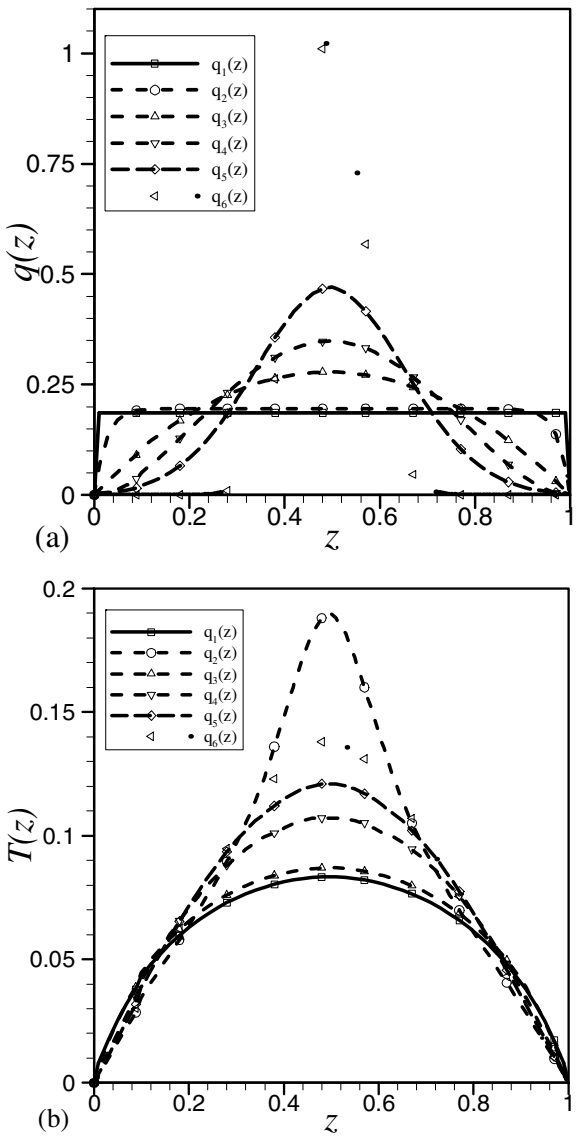

Figure 6 : (a) different profiles of the heat flux defined for the boundary condition (11). (b) surface temperature distribution resulting from the heat flux profiles shown in Fig. 7a.

To argue further we notice that the Marangoni number is defined by the temperature difference between the hottest point on the heater and the melting point at the crystallization front. The actual maximal temperature of the fluid volume, which is obviously located on the side surface, is unknown and can be found only after the whole calculation is done. Presumably, the critical numbers recalculated on the basis of the actual temperature difference, i.e., the difference between the hottest and coldest points of the liquid volume, will be not as different as they are in Figs. 4 and 5.

To check the above assumption we perform the following series of calculations. First, to define a characteristic example, we take the material heating parameters for the floating zone growth of silicon from Munakata & Tanasawa (1999), i.e., Pr=0.011 and Rd=0.00602, and calculate the critical Marangoni number for the radiation boundary condition (8) with $\hat{T}_m = 0$ and $\hat{T}_{heater} = 1$. This calculation yields Mn_{cr}=4.06×10^4. Recalculating the dimensional temperatures using the thermophysical properties of silicon and taking into account that its melting temperature is T_m=1700K, we estimate the heater temperature to be T_{heater} ≈2500K, which is a realistic value. After the computation of Mn_{cr} is done we calculate the Nusselt number at the side surface of the liquid zone

$$Nu = \frac{1}{A}\int_0^A \left[\frac{\partial T}{\partial r}\right]_{r=1} dz \qquad (19)$$

Table 3 : Results for calculations with different heating profiles

$q(z)$	$Mn_{cr}\times10^{-4}$	T_{max}	$q_{\max}=\left[\partial T/\partial r\right]_{\max}$	Nu	$\tilde{T}_{heater}(K)$	$Mn_{eff}\times10^{-4}$
0.1864	3.98	0.083	0.186	0.186	2507	4.05
$0.1953\left[1-\left(1-(1-2z)^{20}\right)\right]$	3.97	0.087	0.195	0.186	2567	4.05
$1.1184z(1-z)$	3.40	0.107	0.279	0.186	3041	4.08
$0.3495\left[1-\left(1-(1-2z)^{2}\right)\right]^{2}$	1.96	0.121	0.349	0.186	3361	4.12
$0.4710\exp\left[-5(1-2z)^{2}\right]$	1.32	0.139	0.471	0.186	3819	4.16
$1.0516\exp\left[-25(1-2z)^{2}\right]$	1.01	0.190	1.052	0.186	5270	4.33

For the calculation described above we obtain Nu=0.1864. Now, we define a series of heat flux profiles for the boundary condition (9) as

$$\begin{aligned} q_1(z) &= 0.1864 \\ q_2(z) &= 0.1953\left[1-\left(1-(1-2z)^{20}\right)\right] \\ q_3(z) &= 1.1184z(1-z) \\ q_4(z) &= 0.3495\left[1-\left(1-(1-2z)^{2}\right)\right]^{2} \\ q_5(z) &= 0.4710\exp\left[-5(1-2z)^{2}\right] \\ q_6(z) &= 1.0516\exp\left[-25(1-2z)^{2}\right] \end{aligned} \tag{20}$$

All these profiles are shown in Fig.6a. The amplitudes of the functions $q_i(z)$ are chosen such that $Nu_i = \int_0^1 q_i(z)\,dz = 0.1864$. We start from the constant heat flux q_1. The profile q_2 vanishes at z=0 and 1 but remains almost constant far from the end points. It is almost equivalent to the profile q_1, but removes the discontinuities of the thermocapillary boundary condition (5) for $\partial v_z/\partial r$ at the end points. The profile q_3 is the same as was used by Walker et al. (2003). The three last profiles are taken from Bennacer et al. (2002) with the amplitudes adjusted to keep the Nusselt number unchanged.

Results of the calculations with the different heat flux profiles (20) are shown in Table 3. For each of the profiles we calculate the critical value of Mn, which is shown in the second column of Table 3. When the critical point is calculated the resulting surface temperature is used for the further evaluations. The resulting surface temperature profiles are shown in Fig. 6b. The maximal temperature T_{max} and the maximal values of the heat flux $q_{\max}=\left[\partial T/\partial r\right]_{\max}$ at the surface are reported in Table 3. On the basis of T_{max} and the thermophysical properties of molten silicon we can estimate also the maximal temperature of the heater, which is also reported in Table 3. It is seen that when the boundary heat flux sharpens so that it grows in the middle and reduces towards the ends the maximal surface temperature grows (cf. Figs. 6a and 6b and the 3^{rd} and 4^{th} columns of Table 3). The maximal heater temperature also grows, so that it reaches an unrealistic value of 5270K for the heat flux profile q_6. This means that in this case when the flow reaches the critical point and undergoes the axisymmetry – three-dimensional transition, a too sharp profile cannot be a good modeling representation of the correct radiative boundary condition modeling. However, it still can be used to elaborate the following result.

Using the calculated maximal surface temperature we rescale the calculated critical number Mn_{cr} by the actual temperature difference of the liquid volume, i.e.,

$$Mn_{eff} = Mn_{cr}\frac{T_{\max}-\widehat{T}_m}{\hat{T}_{heater}-\widehat{T}_m}. \tag{21}$$

Note, that Ma_{eff}=$Mn_{eff}Pr$ is the actual Marangoni number, which one would define considering the surface temperature profiles shown in Fig. 7b. The values of Mn_{eff} are shown in the last column of Table 3. For all the heat flux profiles they differ slightly, grow slowly with the sharpening of profiles, but at the same time remain close to the value of Mn_{eff}=4×10^4. In general, the values of Mn_{eff} vary negligibly as compared to the values of Mn_{cr}. Taking into account, that all the heat flux profile are characterized by the same Nusselt number we reach the following conclusion: the three-dimensional thermocapillary instability inside the liquid zone considered is

defined mainly by the integral amount of heat supplied through the surface and is almost independent of the way the heat is supplied.

5 Concluding remarks

The three-dimensional instability of undeformable floating zones heated from the side was carried out for the fixed zone aspect ratio $A = 1$ and the Prandtl number varied between 0 and 0.1. The primary instability of initially axisymmetric thermocapillary flows was found to take place due to three-dimensional perturbations in all the cases considered. It was shown that for $A = 1$ and small Prandtl numbers the instability sets in due to the azimuthal mode with the wavenumber $k = 3$. With the increase of the Prandtl number the primary instability switches to the azimuthal mode with $k = 1$ and with further increase of Pr to the mode with $k = 2$.

We have shown that the axisymmetric – three-dimensional transition in the laterally heated floating zones takes place in a similar manner for the three types of the heating boundary conditions applied. The thermal radiation boundary condition can be simplified by a linearization or by imposing an axially distributed heat flux under the condition that the total amount of heat supplied through the surface is kept unchanged. This condition seems to be obvious, however such a replacement leads to a redefinition of the Marangoni number, so that resulting critical Marangoni numbers obtained for differently formulated boundary conditions can significantly diverge. This diverging is caused by the necessarily different definition of the characteristic temperature difference in the definition of the Marangoni number, and can be removed by a redefinition of the Marangoni number using the actual calculated temperature difference of the liquid volume. At the same time it is emphasized that the values of the Prandtl number at which the different most unstable modes replace each other can differ significantly for different types of the boundary conditions (Fig. 5), which means that the simplification of the boundary conditions can lead to a wrong most unstable mode and should be done with necessary precautions.

Acknowledgement: This research was supported by the Asher Space Research Institute, Technion (to P. Bar-Yoseph). The authors would like to acknowledge the use of computer resources belonging to the High Performance Computer Unit, a division of the Inter University Computer Center, which is a consortium formed by research universities in Israel.

References

Albanese, C.; Carotenuto, L.; Castagnolo, D.; Ceglia, E.; Monti, R.; (1995): An investigation of the "onset" of oscillatory Marangoni flow. *Adv. Space Res.,* vol. 16, No. 7, pp. 87-94.

Bennacer, R.; Mohamad, A.A.; Leonardi, E. (2002): The effect of heat flux distribution on thermocapillary convection in a side-heated liquid bridge, *Numer. Heat Transfer, Part A*, vol. 41, pp. 657-671.

Chen, G.; Lizee, A.; Roux, B. (1997): Bifurcation analysis of the thermocapillary convection in cylindrical liquid bridges, *J. Crystal. Growth*, vol. 180, pp. 638-647.

Cröll, A.; Kaiser, Th.; Schweizer, M.; Danilewsky, A.N.; Lauer, S.; Tegeteimer A.; Benz, K.W. (1998): Floating-zone and floating-solution-zone growth of GaSb under microgravity. *J. Cryst. Growth*, vol. 191, pp. 365-376.

Dold, P. (2004): Analysis of microsegregation in RF-heated float zone growth of silicon - comparison to the radiation-heated process. *J. Cryst. Growth*, vol. 261, pp. 1-10.

Gelfgat, A.Yu.; Bar-Yoseph, P.Z.; Solan, A. (2000): Axisymmetry breaking instabilities of natural convection in a vertical Bridgman growth configurations. *Journal of Crystal Growth*, vol. 220, pp. 316-325.

Gelfgat, A.Yu.; Rubinov; A., Bar-Yoseph, P.Z.; Solan, A. (2005): Numerical study of three-dimensional instabilities in a hydrodynamic model of Czochralski growth, *J. Crystal Growth*, vol. 275, pp. e7-e13.

Hibiya, T.; Nakamura, S.; Sumiji, M.; Azami, T. (2002): Non-invasive techniques for observing the surface behavior of molten silicon. *J. Cryst. Growth*, vol. 237-239, pp. 1854-1858.

Hsieh, W.C.; **Lan, C.W.** (1996): Experimental study on floating zone tube growth and comparison with computer simulation. *J. Cryst. Growth*, vol. 165, pp. 447-454.

Imaishi, N.; Yasuhiro, S.; Akiyama, Y.; Yoda, S. (2001): Numerical simulation of oscillatory Marangoni flow in half-zone liquid bridge of low Prandtl number fluid, *J. Cryst. Growth*, vol. 230, pp. 164-171.

Kamotani, Y.; Wang, L.; Hatta, S.; Wang, A.; Yoda, S. (2003): Free surface heat loss effect on oscillatory

thermocapillary flow in liquid bridges of high Prandtl number fluids. *Int. J. Heat Mass Transf.,* vol. 46, pp. 3211-3220.

Kasperski, G.; Batoul, A.; Labrosse, G. (2000): Up to the unsteadiness of axisymmetric thermpocapillary flow in a laterally heated liquid bridge. *Phys. Fluids*, vol. 12, pp. 103-119.

Kimura, H.; Miyazaki, A.; Maiwa, K.; Nakamura, H. (2004): Fluctuation of crystallization at center part of floating molten zone under reduced gravity condition. *Cryst. Res. Technol.,* vol. 39, pp. 117-122.

Kuhlmann, H.C.; Rath, H.J. (1993): Hydrodynamic instabilities in cylindrical thermocapillary liquid bridges. *J. Fluid Mech.,* vol. 247, pp. 247-274.

Lan, C.W.; Chian, J.H. (2001): Three-dimensional simulation of Marangoni flow and interfaces in floating zone silicon crystal growth. *J. Cryst. Growth*, vol. 230, pp. 172-180.

Lan, C.W. (2003): Three-dimensional simulation of floating zone crystal growth of oxide crystals. *J. Cryst. Growth*, vol. 247, pp. 597-612.

Lappa, M.; Savino, R.; Monti, R. (2001): Three-dimensional numerical simulation of Marangoni instabilities in non-cylindrical liquid bridges in microgravity. *Int. J. Heat Mass Transf.,* vol. 44, pp. 1983-2003.

Lappa, M. (2003): Three-dimensional numerical simulation of Marangoni flow instabilities in floating zones laterally heated by equatorial ring. *Phys. Fluids*, vol. 15, pp. 776-789.

Lappa, M. (2004): Fluids, Materials and microgravity: Numerical Techniques and Insights into the Physics. Elsevier, Oxford.

Lappa, M. (2005): Analysis of flow instabilities in convex and concave floating zones heated by an equatorial ring under microgravity conditions. *Computers & Fluids*, vol. 34, pp. 743-770.

Levenstam, M.; Amberg, G.; Winkler, C. (2001): Instabilities in thermocapillary covection in a half-zone at intermediate Prandtl numbers. *Phys. Fluids*, vol. 13, pp. 807-816.

Majima, S.; Nakamura, H.; Otsubo, F.; Kuwahara, K.; Doi, T. (2001): Oscillatory thermocapillary flow in encapsulated liquid column. *Phys. Fluids*, vol. 13, pp. 1517-1520.

Melnikov, D.E.; Shevtsova, V.M.; Legros, J.C. (2005): Route to aperiodicity followed by high Prandtl-number liquid bridge. 1-g case. *Acta Astronautica*, vol. 56, pp. 601-611.

Minakuchi, H.; Okano, Y.; Dost, S. (2004): A three-dimensional numerical simulation of the Marangoni convection occurring in the crystal growth of Si_xGe_{1-x} by the float-zone technique in zero gravity. *J. Cryst. Growth*, vol. 266, pp. 140-144.

Muehlner K.A.; **Schatz, M.F.; Petrov, V.; McCormick, W.D.; Swift, J.B.; Swinney, H.L.** (1997): Observation of helical traveling-wave convection in a liquid bridge. *Phys. Fluids*, vol. 9, pp. 1850-1852.

Munakata, T.; **Tanasawa, I.** (1999): Study on silicon melt convection during the RF-FZ crystal growth process. II. Numerical investigation. *J. Cryst. Growth*, vol. 206, pp. 27-36.

Nishimura, M.; Ueno, I.; Nishino, K.; Kawamura, H. (2005): 3D PTV measurements of oscillatory thermocapillary convection in half-zone liquid bridge. *Exp. Fluids*, vol. 38, pp. 285-290.

Preisser, F.; Schwabe, D.; Scharmann A.; (1983): Steady and oscillatory thermocapillary convection in columns with free cylindrical surface. *J. Fluid Mech.,* vol. 126, pp. 545-567.

Rubinov, A.; Erenburg, V.; Gelfgat, A.Yu.; Kit, E.; Bar-Yoseph, P.Z.; Solan, A. (2004): Three-dimensional instabilities of natural convection in a vertical cylinder with partially heated sidewalls. *J. Heat Transfer,* vol. 126, pp. 586-599.

Shen, Y.; Neitzel, G.P.; Jankowsky, D.F.; Mittelmann, H.D. (1990): Energy stability of thermocapillary convection model of the float zone crystal-growth process. *J. Fluid Mech.,* vol. 217, pp. 639-660.

Sumner, L.B.S.; Neitzel, G.P.; Fontaine, J.-P.; Dell'Aversana, P. (2001): Oscillatory thermocapillary convection in liquid bridges with highly deformed free surfaces: experiments and energy stability analysis. *Phys. Fluids*, vol. 13, pp. 107-120.

Walker, J.S.; Martin Witkowsky, L.; Houchens, B.C. (2003): Effects of a rotating magnetic field on the thermocapillary instability in the floating zone process. *J. Cryst. Growth*, vol. 252, pp. 413-423.

Wanshura, M.; Shevtsova, V.M.; Kuhlmann, H.C.; Rath, H.J. (1995): Convective instability in thermocapillary liquid bridges, *Phys. Fluids*, vol. 7, pp. 912-925.

Yang, Y.K.; Kou, S. (2001): Temperature oscillation in a tin liquid bridge and critical Marangoni number dependency on Prandtl number. *J. Cryst. Growth*, vol. 222, pp. 135-143.

Yasuhiro, S.; Li, K.; Imaishi, N.; Akiyama, Y.; Natsui, H.; Matsumoto, S; Yoda, S. (2004): Oscillatory Marangoni flow in half-zone liquid bridge in molten tin. *J. Cryst. Growth*, vol. 266, pp. 152-159.

Zeng, Z.; Mizuseki, H.; Simamura, K.; Fukuda, T.; Higashino, K.; Kawazoe, Y. (2001): Three-dimensional oscillatory thermocapillary convection in liquid bridge under microgravity. *Int. J. Heat Mass Transf.,* vol. 44, pp. 3765-3774.